Nuclear Materials and Energy 000 (2017) 1–5

Contents lists available at ScienceDirect

Nuclear Materials and Energy

journal homepage: www.elsevier.com/locate/nme

Observation and particle simulation of vaporized W, Mo, and Be in PISCES-B plasma for vapor-shielding studies

K. Ibano[a,*], D. Nishijima[b], J.H. Yu[b], M.J. Baldwin[b], R.P. Doerner[b], T. Takizuka[a], H.T. Lee[a], Y. Ueda[a]

[a] Graduate School of Engineering, Osaka University, E6-518 2-1 Yamada-oka, Japan
[b] Center for Energy Research, University of California, San Diego, La Jolla, CA.92093-0417, USA

ARTICLE INFO

Article history:
Received 15 July 2016
Revised 3 December 2016
Accepted 18 January 2017
Available online xxx

Keywords:
Vapor shielding
Plasma-vapor interaction
Particle-in-cell simulation

ABSTRACT

Interactions of Tungsten (W), Molybdenum (Mo), and Beryllium (Be) vapors with a steady-state plasma were studied by the PISCES-B liner plasma experiments as well as Particle-In-Cell (PIC) simulations for the understanding of vapor-shielding phenomena. Effective cooling of the plasma by laser-generated Be vapor was observed in PISCES-B. On the other hand, no apparent cooling was observed for W and Mo vapors. The PIC simulation explains these experimental observations of the difference between low-Z and high-Z vapors. Decrease of electron temperature due to the vapor ejection was observed in case of a simulation of the Be vapor. As for the W vapor, it was found that the plasma cooling is localized only near the wall at a higher electron density plasma ($\sim 10^{19}$ m^{-3}). On the other hand, the appreciable plasma cooling can be observed in a lower density plasma ($\sim 10^{18}$ m^{-3}) for the W vapor.

1. Introduction

For ITER and post-ITER tokamak fusion reactors, the erosion of wall materials due to pulsed heat loads by ELMs and disruptions is one of the most serious concerns [1]. These heat loads cause significant erosion via melting and vaporization of the metallic walls. Meanwhile, the vapors generated from the surface interact with the incoming plasma-flux, and this vapor-plasma interaction can dissipate the heat flux to the wall via radiation cooling and ionization energy loss. This phenomenon is known as “vapor shielding” and has been studied extensively by experiments in plasma-gun devices [2,3] and linear devices [4]. Vapor shielding phenomena for low-Z materials were well observed in these experiments. However, apparent observation of vapor shielding of high-Z materials has not been achieved yet. In this paper, instead of using the high-density plasma gun to generate vapor directly by the plasma flux, pulsed laser irradiations were used for the vapor generation. Interaction of produced vapor with background plasma was studied in the PISCES-B steady-state linear plasma device. Although the observation of vapor shielding effects via changes of surface temperature and heat flux is difficult due to the small area of laser irradiation spots, use of the laser heat loads makes it possible to control vapor amounts independently of the incoming plasma parameters. Observing line emissions from the vapor neutrals using a fast-camera and spectrometer, the plasma energy dissipation due to the plasma-vapor interaction was examined for vapor from Tungsten (W), Molybdenum (Mo), and Beryllium (Be) sample targets.

As well as the experimental studies, numerical approaches have been taken by using MHD fluid models for the plasma and vapor motions [5,6]. These fluid models demonstrated the importance of radiation cooling for the vapor shielding. Their results agreed well with the experimental observations of the vapor shielding by low-Z materials. On the other hand, a hypothesis given in Refs. [5,6] suggested that kinetic effects in the sheath and pre-sheath regions may play significant roles for the vapor shielding by the high-Z materials and that fluid modeling is not enough for this study. It is already known that ejected high-Z particles tend to be re-deposited promptly to the surface due to their large gyro radius and the pre-sheath electric field. Thus, understanding of their kinetic behavior in the vicinity of the wall is crucial in the vapor-plasma interaction study. We have been developing a particle-in-cell (PIC) code to examine these kinetic effects on the vapor shielding [7]. Explanation on experimental observations about difference between low-Z and high-Z metals were obtained from the PIC simulation and discussed in Section 4.

* Corresponding author.
E-mail addresses: kibano@gmail.com, kibano@eei.eng.osaka-u.ac.jp (K. Ibano).

http://dx.doi.org/10.1016/j.nme.2017.01.016

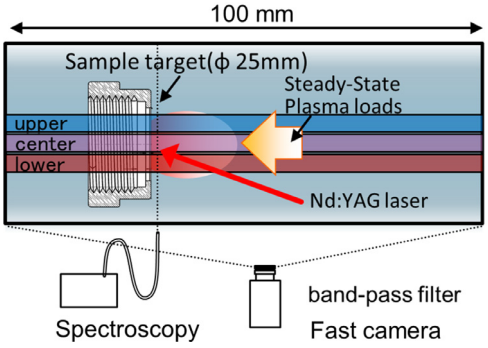

Fig. 1. Schematic view of the experimental set-up at the PISCES-B device.

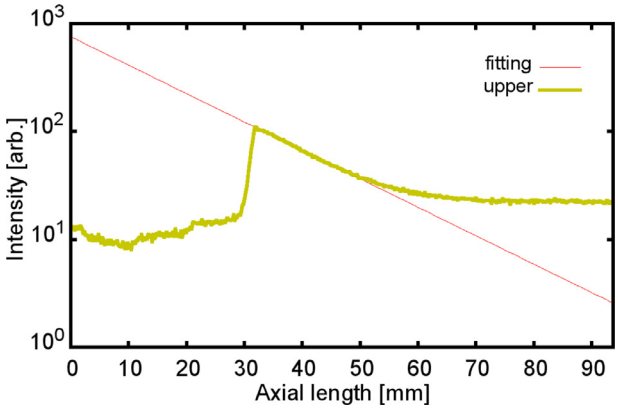

Fig. 2. Axial profile of W I line intensity. The profile is fitted well by an exponential curve with decay length of 20 mm (red line). (For interpretation of the references to color in this figure legend, the reader is referred to the web version of this article.)

2. Experimental procedure

PISCES-B is a linear plasma device, which confines a LaB_6 cathode generated arc plasma by the axial magnetic fields. The experimental set-up is shown in Fig. 1. In this study, the targets were irradiated with He or Ar plasma, the typical parameters of which were electron temperature $T_e \sim 6.5$ eV, electron density $n_e \sim 10^{19}$ m^{-3} and ion flux $\Gamma_i \sim 10^{23}$ m^{-2}s^{-1}. Ar plasma was only applied to a W target in order to observe an optical decay length of its sputtered particles. Then, pulsed loads from a Nd:YAG laser (NEC M801C, 1064 nm wavelength) were simultaneously applied to the target surface. The maximum laser energy from the laser source was 50 J and the duration was 10–20 ms with a square-wave pulse. However, the amount of laser energy transferred to the surface is much smaller due to the transport loss. The laser beam diameter on the target surface was about 2 mm. Several laser shots were applied for a target specimen, while each laser spot was moved onto a non laser-irradiated area.

Each target sample was a circular plate with 25 mm diameter and 1.5 mm and thickness was clamped between a forced air-cooled cupper base and a screwed Ta holder. The target temperature was monitored by a thermocouple located in the center of the cupper base. The target temperature was kept below the surface fuzz growing threshold [8]. During the steady-state plasma loads, a negative bias voltage up to −120 V was applied on the entire target holder. This bias voltage was chosen so that the surface sputtering particles can be observed and compared with the evaporated particles by their optical emissions. The ion energy would be similar or higher in cases of transient events. [9]

A high-speed camera (phantom v710) was used to observe the emitted light from vapor particles and from the background plasma. The camera recorded light intensities from area of 100 × 50 mm by 512 × 256 pixels in 12 bit data and at 500–5000 frames per seconds. Optical filters were set in front of the camera lens so that the line emissions from neutral particles of interest were recorded; 430.2 nm with a full width at half maximum FWHM of 3 nm for WI, 550.0 nm (10 nm FWHM) for MoI, 457.9 nm (3 nm FWHM) for BeI, and 667.8 nm (10 nm FWHM) for HeI. In addition to the high-speed camera observation, a spectroscopic measurement was also taken in front of the target. A two channel spectrometer (Avantes, AvaSpec-DUAL) was used and radiation spectra within 410–660 nm wave-length were recorded at every 1.5 ms.

Pictures recorded by the high-speed camera were analyzed frame by frame using ImageJ [10]. Axial intensity profiles were obtained by averaging intensities of 10–20 pixels over the vertical direction. In order to avoid effects of the continuous spectrum radiation from secondary electron emission (SEE), profiles for three different locations (upper, centers and lower) were examined (see Fig. 1). We assumed that the SEE disturbs the observation mainly at the center region, while it does not strongly disturb the other two regions. An exponential fit worked well with these profiles, and the 1/e decay length from the maximum intensity was obtained (Fig. 2). The decay length of the first line intensity roughly represents the ionization mean free path. Temporal evolution of the decay length was then calculated for every intensity profile data. Smoothed lines were added for periodic oscillating temporal evolutions of these maximum intensity values and the decay lengths. These oscillations arise from the plasma rotation due to the radial electric field and axial magnetic field.

3. Optical observations of vaporized particles in PISCES-B steady-state plasma

Fig. 3(a) and (b) show results from experiments using a W target irradiated by Ar plasma loads. The maximum intensity of the WI line emission gradually increases during the laser irradiation and rapidly returns to the original value after the pulse. On the other hand, the decay length decreases during the laser irradiation. This decreasing decay length is simply explained by the ejection energy difference of sputtered and vaporized particles. During the laser irradiation, the vaporized particles dominate the light intensity as shown in Figs. 3(a) and 4(a). As a result, the intensity peak position became apparently shifted to the surface direction because of the slower velocity of vaporized particles compared with sputtered particle. Accordingly, the decay length became shorter. Similar results were obtained from a Mo target irradiated by He plasma as seen in Fig. 4(a) and (b).

In contrast, an increase in the decay length during the laser irradiation was observed for the Be target under the He plasma loads, as shown in Fig. 5(a). Comparing 16 J (Fig. 5(a)) and 9 J (Fig. 5(b)) laser shots, it is noted that the increasing decay length was not observed for a lower energy shot with 9 J. At the same time, spectroscopic results showed that the Be II line intensity increases with the increasing the laser energy (Fig. 6(a)). The He I line intensity dropped only with the highest laser energy of 16.7 J. (Fig. 6(b)) Neither the increasing decay length nor the decreasing line radiation of the background plasma were observed for experiments with smaller laser energy irradiation on the same Be sample. The photon emission coefficient of the He I line and the ionization rate coefficients are a strong function of T_e. According to the OPEN-ADAS library [11], these coefficients at 6 eV is an order of magnitude higher than that of 3 eV. Here, the increasing Be II line intensity indicates increasing n_e due to ionization reaction. Higher n_e would increase the He I line intensity and decrease the decay length, but the experimental observations show in reverse. Thus, the plasma cooling by the emitted Be vapor is the main candidate

Please cite this article as: K. Ibano et al., Observation and particle simulation of vaporized W, Mo, and Be in PISCES-B plasma for vapor-shielding studies, Nuclear Materials and Energy (2017), http://dx.doi.org/10.1016/j.nme.2017.01.016

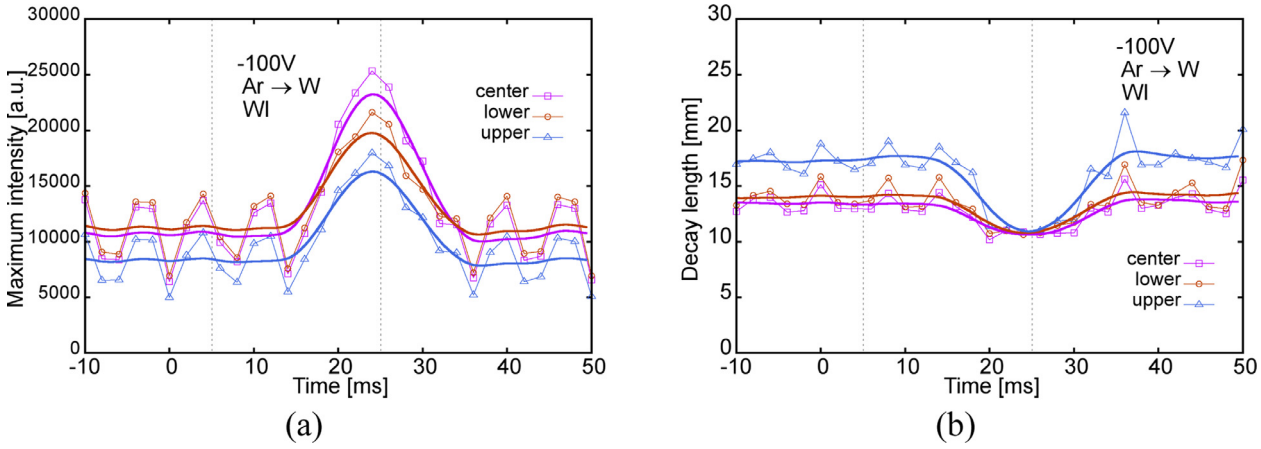

Fig. 3. Time evolution of (a) maximum intensity and (b) decay length of W I line intensity in Ar plasma with 48 J laser irradiation. Laser irradiation was applied during 5 ms–25 ms between vertical lines in the figures.

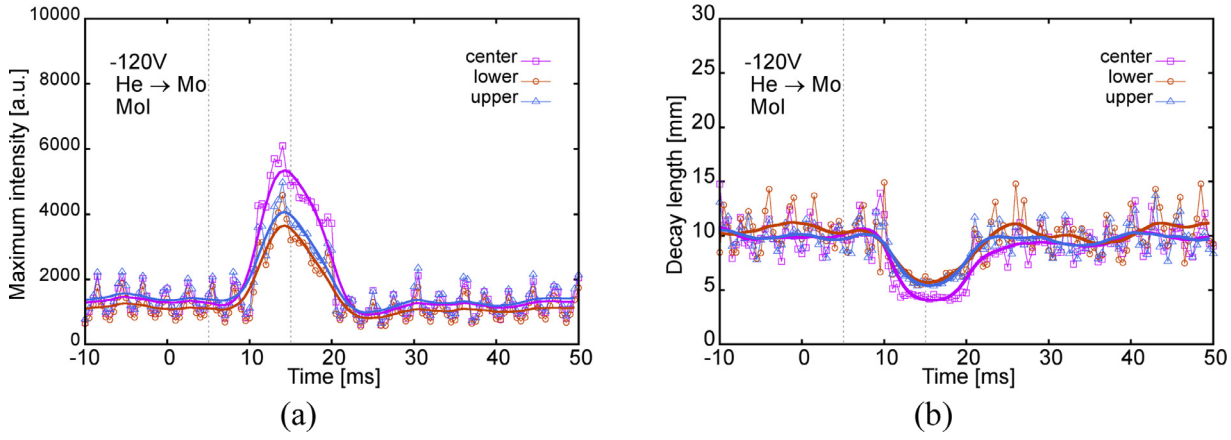

Fig. 4. Time evolution of (a) maximum intensity and (b) decay length of Mo I line intensity in He plasma with 48 J laser irradiation. Laser irradiation was applied during 5 ms–15 ms between vertical lines.

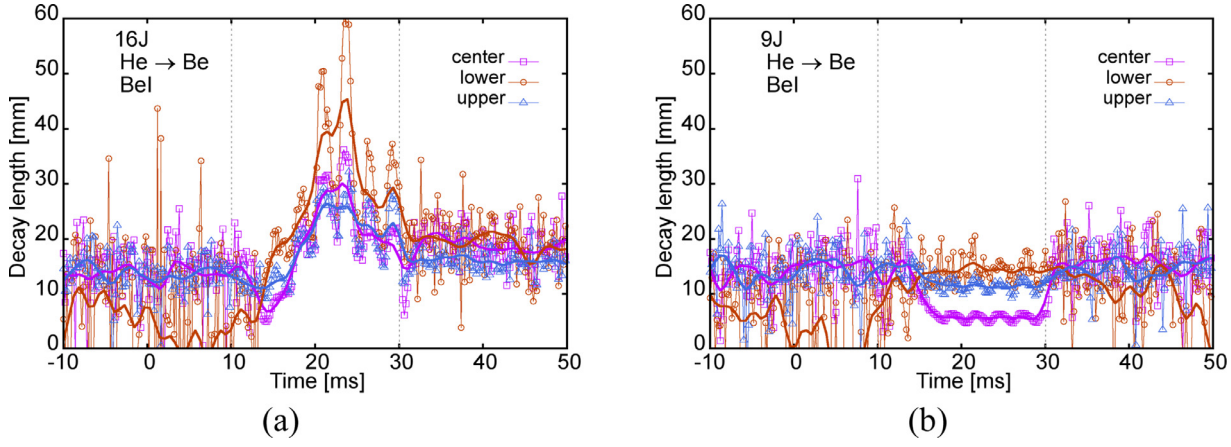

Fig. 5. Time evolution of decay length of Be I line intensity in He plasma with (a) 16 J and (b) 9 J laser irradiation. Laser irradiation was applied during 10 ms–30 ms between vertical lines.

for the increasing decay length as mentioned in Ref. [12]. The He I line intensity during the W irradiation was also shown in Fig. 6(b).As this figure and Fig. 4 show, these cooling effects were not observed in cases of W and Mo targets even for the higher laser energy irradiation up to 50 J. This experimental observation of difference between low-Z metal (Be) and high-Z metals (Mo, W) motivated following simulation study.

4. PIC simulations

The PIC code used in this study treats one dimensional in geometry and three velocity components (1d3v). Ionization and recombination reactions are treated with the Monte-Carlo method based on their atomic cross sections obtained from the OPEN-ADAS library [11]. Radiation cooling power as well as line intensities are also calculated using the library. A weighted particle

Please cite this article as: K. Ibano et al., Observation and particle simulation of vaporized W, Mo, and Be in PISCES-B plasma for vapor-shielding studies, Nuclear Materials and Energy (2017), http://dx.doi.org/10.1016/j.nme.2017.01.016

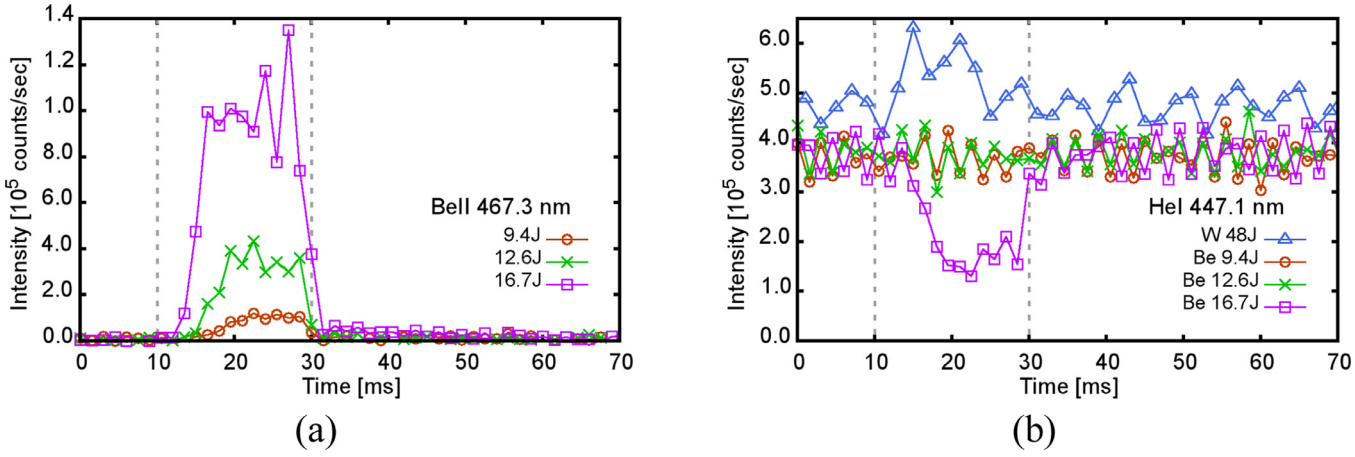

Fig. 6. Time evolution of (a) Be II line and (b) He I line intensities in He plasma with 9 J (brown circle), 12 J (green cross) and 16 J (violet square) laser irradiations for Be and 48 J laser irradiations for W (blue triangle) measured by the spectroscopy. Laser irradiation was applied during 10 ms–30 ms between vertical lines. (For interpretation of the references to color in this figure legend, the reader is referred to the web version of this article.)

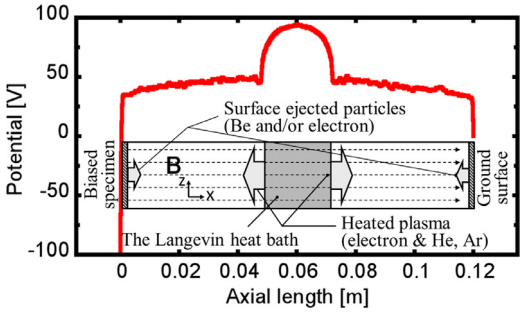

Fig. 7. Potential profile of the simulated PISCES-B plasma in a steady state with schematic model used for the Particle-In-Cell simulation of the PISCES-B plasma. The left boundary was set as a biased target $V_b = -100$ V.

technique is used for the impurity particles. In the PIC simulation, super particles which represent more than billions of real particles are treated. And numbers of the representing real particles are called as weighting of the super particle which is usually uniform for entire calculations. Using the weighted particle technique, weighting is no longer a constant for all particles but a particle-dependent parameter. Thus, the statistical errors of the lower-density impurity particle can be minimized by using enough number of super-particles with smaller weighting compared with background plasma and vice versa. Further details of this code and its ionization/recombination scheme are described in Ref. [9].

Using this PIC code, a calculation domain as included in Fig. 7 is constructed for the simulation. In this calculation domain, the central region was treated as a heating region, the right boundary was treated as a wall with the ground potential, and the left boundary was treated as a biased target boundary. Particles reaching to the boundaries were recycled from the surface or refuel into the system from the central region in order to conserve the particle amounts in the system. Using this simulation domain, we simulated a PISCES-B He plasma with $T_e = 6.5$ eV and $n_e = 2 \times 10^{19}$ m^{-3} in a magnetic field along x direction ($B_x = 0.015$T and $B_z = 0$). An example of the simulated potential profile for the steady-state condition is shown also in Fig. 7. The actual device has a radial distribution of potential profile, and these 2D features cannot be included in this 1D simulation. However, the Debye sheath potential drop in the vicinity of boundary as well as pre-sheath potential gradient is well simulated.

Once simulated plasma reaches a steady-state condition, a certain amount of impurity neutral particles were emitted from the left boundary. The energy of emitted impurities was kept at 0.1 eV, and the emission angle was given with the cosine distribution. Behavior of impurity particles and their influence to the background plasma were examined for different flux of impurity emissions.

Simulation results of Be and W impurity emission were compared in Fig. 8. In these figures, profiles of electron temperature, total radiation power, total impurity density, and impurity neutral density at 12 μs after the impurity ejection are plotted. A clear decrease of the electron temperature can be observed up to $x > 1$ cm for the Be emission. In contrast, the influence of the W emission is localized in the vicinity of the surface $x << 1$ cm. We see that the most of emitted W particles are ionized shortly after the emission, and then they are soon pulled back by the sheath and pre-sheath electric field to the walls before contributing to the plasma cooling. Since a W atom is about 20 times heavier and ionization rate coefficient is 2 times larger than Be atom, its ionization mean free path ($\frac{v_{neutral}}{n_e \langle \sigma v_e \rangle} \propto \{\sqrt{m_{neutral}} \langle \sigma v_e \rangle\}^{-1}$) is about 9 times shorter.

In the experiments shown in Section 3, no apparent vapor shielding behavior was observed for the W sample even for the higher intensity laser shots. The vapor pressure and the ejection rate of W is significantly smaller than the Be. The ejection rate of the W vapor by the 50 J laser irradiation was evaluated as $\sim 10^{23}$ atoms/m^{2}s. In this measurement, laser irradiations under D plasma loads were repeated for 30 times and mass loss was measured. At the same time, the PIC calculation indicated that ejections of W particles did not result in the apparent heat-flux dissipation even for the similar or higher ejection rate compared with Be up to $\sim 10^{23}$ atoms/m^{2}s. This simulation results also explained the absence of the vapor shielding of W specimens in the PISCES-B experiments.

It was indicated by the PIC simulations that the main difficulty for the observation of W vapor shielding is its short ionization mean free path. The electron density n_e varies the sheath thickness d_{sh} with $\sim 1/n_e{}^{1/2}$ while the ionization mean free path l_{iz} with $\sim 1/n_e$. Thus, the heat-flux dissipation by W vapor impurity could be observed in lower-n_e experiments, i.e., $l_{iz} >> d_{sh}$. Fig. 9 shows PIC simulation results of profiles of electron temperature and tungsten neutral density at 12 μs after 10^{23} atoms/m^{2}s ejection as a function of background electron density. Electron temperature drops are observed in simulation of the lower plasma density ($<10^{18}$ m^{-3}). Thus, the plasma cooling by the W vapor would be observable in experiments with $<10^{18}$ m^{-3} density plasma.

Please cite this article as: K. Ibano et al., Observation and particle simulation of vaporized W, Mo, and Be in PISCES-B plasma for vapor-shielding studies, Nuclear Materials and Energy (2017), http://dx.doi.org/10.1016/j.nme.2017.01.016

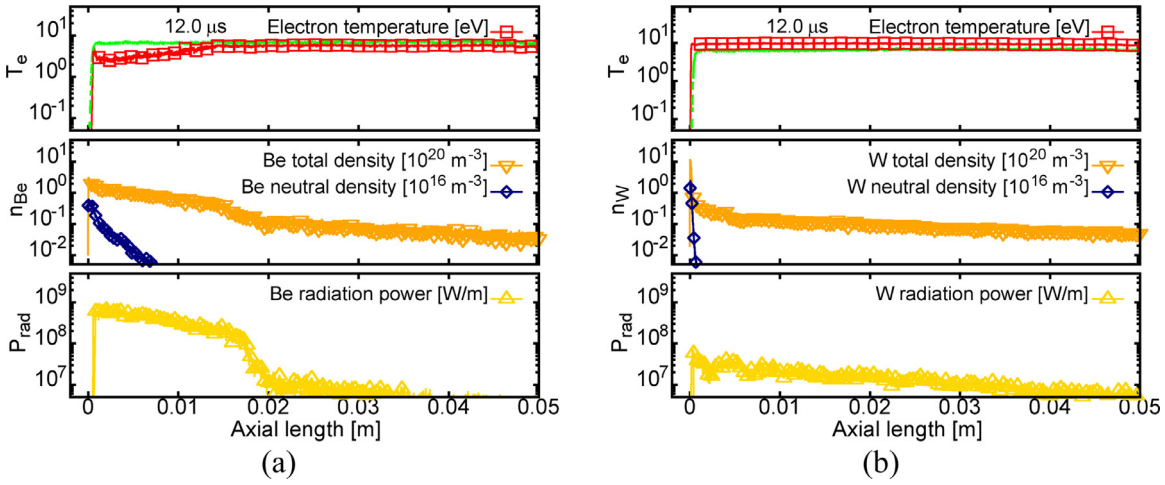

Fig. 8. Simulated profiles of electron temperature (red), total impurity density (orange), and impurity neutral density (navy) and total impurity radiation power (yellow) 12 μs after the 2×10^{23} atoms/m^{2}s impurity ejection of (a) Be and (b) W in the 10^{19} m^{-3} electron density plasma. Green line indicates T_e profile at the steady-state before the impurity ejection. (For interpretation of the references to color in this figure legend, the reader is referred to the web version of this article.)

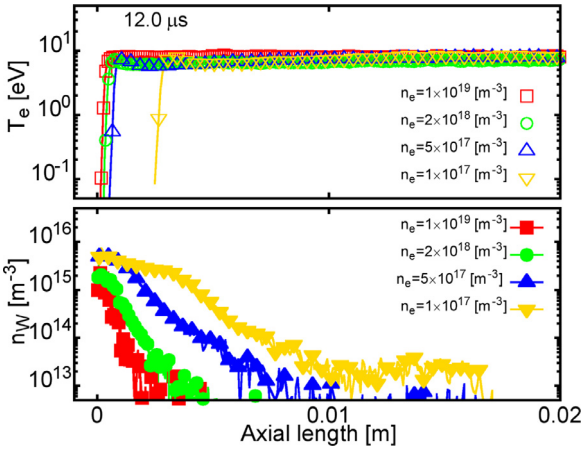

Fig. 9. Simulated profiles of T_e (blank) and n_n (filled) 12 μs after the impurity ejection of 2×10^{23} atoms/m^{2}s in the 10^{17} m^{-3} ~ 10^{19} m^{-3} electron density plasma.

5. Summary

W, Mo, and Be sample targets were irradiated by steady-state He or Ar plasma in the PISCES-B device. Simultaneous irradiation by milliseconds pulsed Nd:YAG laser shots generated surface-originated vapor. As Be vapor increased with higher laser intensities, decay lengths of BeI line radiation increase. At the same time, the significant Be vapor generation resulted in the plasma cooling near the surface, which was indicated by decreasing HeI line intensity and increasing BeII intensity. No apparent plasma cooling was observed with experiments of W and Mo target samples.

Effects of kinetic motions of the ejected impurities in the vicinity of the wall were analyzed by the PIC simulations in order to explain this difference between low-Z and high-Z metals. Drops in the electron temperature within >1 cm from the wall were observed in a simulation of the 2×10^{23} Be/m^{2}s ejection into the 10^{19} m^{-3} electron density plasma. Comparing the same amounts of Be and W ejections from the walls, it was found that effects from the ejected W particles were localized in the vicinity of the wall. Re-deposition due to its short ionization mean free path and the sheath potential drop prevents W particles from cooling the background plasma. In contrast, the effective plasma cooling behavior was observed for Be cases. It was also indicated by the PIC simulation that plasma cooling by W vapor can be observed if lower density ($<10^{18}$ m^{-3}) steady-state plasma is used in experiments.

Acknowledgement

This work was partly supported by Japan / U. S. Cooperation in Fusion Research and Development, JSPS KAKENHI Grant Number 25249132, and by the US DOE Grant: DE-FG02-07ER54912.

References

[1] G. Federici, A.R. Raffray, J. Nucl. Mater. 244 (1997) 101–130.
[2] V.I. Tereshin, A.N. Bandura, O.V Byrka, et al., Plasma Phys. Control. Fusion 49 (2007) A231–A239.
[3] I. Sakuma, Y. Kikuchi, Y. Kitagawa, et al., J. Nucl. Mater. 463 (2015) 233–236.
[4] G.G. van Eden, T.W. Morgan, D.U.B. Aussems, et al., Phys. Rev. Lett. 116 (2016) 135002.
[5] A. Hassanein, Fusion Eng. Des. 60 (2002) 527–546.
[6] H. Wurz, I. Landman, B. Bazylev, et al., J. Nucl. Mater. 233 (1996) 798–802.
[7] K. Ibano, S. Togo, T.L. Lang, et al., Plasma Phys. (2016) 56.
[8] M.J. Baldwin, R.P. Doerner, Nucl. Fusion. 48 (2008) 35001.
[9] A.W. Leonard, N. Asakura, J.A. Boedo, et al., Plasma Phys. Control. Fusion. 48 (2006) A149–A162.
[10] C.A. Schneider, W.S. Rasband, K.W. Eliceiri, Nat. Methods. 9 (2012) 671–675.
[11] H.P. Summers, M.G. O'Mullane, Atomic data and modelling for fusion: the ADAS project, in: AIP Conference Proceeding, 2011, pp. 179–187.
[12] S. Takamura, Y. Uesugi, Nucl. Fusion (2015) 55.